



HAL
open science

An improved Lagrangian model for the time evolution of nonlinear surface waves

Charles-Antoine Guérin, Nicolas Desmars, Stéphan T. Grilli, Guillaume Ducrozet, Yves Perignon, Pierre Ferrant

► To cite this version:

Charles-Antoine Guérin, Nicolas Desmars, Stéphan T. Grilli, Guillaume Ducrozet, Yves Perignon, et al.. An improved Lagrangian model for the time evolution of nonlinear surface waves. *Journal of Fluid Mechanics*, 2019, 876, pp.527-552. 10.1017/jfm.2019.519 . hal-02310305

HAL Id: hal-02310305

<https://hal.science/hal-02310305>

Submitted on 2 Sep 2020

HAL is a multi-disciplinary open access archive for the deposit and dissemination of scientific research documents, whether they are published or not. The documents may come from teaching and research institutions in France or abroad, or from public or private research centers.

L'archive ouverte pluridisciplinaire **HAL**, est destinée au dépôt et à la diffusion de documents scientifiques de niveau recherche, publiés ou non, émanant des établissements d'enseignement et de recherche français ou étrangers, des laboratoires publics ou privés.

An improved Lagrangian model for the time evolution of nonlinear surface waves

Charles-Antoine Guérin^{1†}, Nicolas Desmars², Stéphan T. Grilli³,
Guillaume Ducrozet², Yves Perignon² and Pierre Ferrant²

¹Université de Toulon, Aix-Marseille Université, IRD, CNRS-INSU, Mediterranean Institute of Oceanography (MIO UM 110), 83957 La Garde, France

²Ecole Centrale Nantes, LHEEA Res. Dept. (ECN and CNRS), Nantes, France

³Department of Ocean Engineering, University of Rhode Island, Narragansett, RI 02882, USA

(Received ?; revised ?; accepted ?. - To be entered by editorial office)

Key words: Will be entered by the editorial office.

Accurate real-time simulations and forecasting of phase-resolved ocean surface waves require nonlinear effects, both geometrical and kinematic, to be accurately represented. For this purpose, wave models based on a Lagrangian steepness expansion have proved particularly efficient, as compared to those based on Eulerian expansions, as they feature higher-order nonlinearities at a reduced numerical cost. However, while they can accurately model the instantaneous nonlinear wave shape, Lagrangian models developed to date cannot accurately predict the time-evolution of even simple periodic waves. Here, we propose a novel and simple method to perform a Lagrangian expansion of surface waves to second-order in wave steepness, based on the dynamical system relating particle locations and the Eulerian velocity field. We show that a simple redefinition of reference particles allows to correct the time-evolution of surface waves, through a modified nonlinear dispersion relationship. The resulting expressions of free surface particle locations can then be made numerically efficient by only retaining the most significant contributions to second-order terms, i.e., Stokes drift and mean vertical level. This results in a hybrid model, referred to as “Improved Choppy Wave Model” (ICWM) [with respect to Noguier et al.’s (2009) ‘Choppy Wave’ Model for nonlinear gravity waves. *J. Geophys. Res.: Oceans* **114** (C9)], whose performance is numerically assessed for long-crested waves, both periodic and irregular. To do so, ICWM results are compared to those of models based on a High-Order Spectral method and classical second-order Lagrangian expansions. For irregular waves, two generic types of narrow- and broad-banded wave spectra are considered, for which ICWM is shown to significantly improve wave forecast accuracy as compared to other Lagrangian models; hence, ICWM is well-suited to provide accurate and efficient short-term ocean wave forecast (e.g., over a few peak periods). This aspect will be the object of future work.

1. Introduction

A wide variety of ocean engineering or oceanographic applications require real-time data on phase-resolved ocean surface waves, typically for mildly- to strongly-nonlinear irregular sea-states (in terms of a total wave steepness ϵ). For instance both real-time ocean waves as well as their short term forecast are required for predicting and controlling

† Email address for correspondence: guerin@univ-tln.fr

the motion of vessels (Perez 2006; Dannenberg *et al.* 2010), or wave power harvesting devices, e.g., in order to optimize loading/offloading operations, seakeeping/stability (e.g., for small unmanned surface vehicles) (Grilli *et al.* 2011; Noguier *et al.* 2014), or wave energy capturing (Babarit & Clément 2006).

Real-time, phase-resolved, ocean waves can be reconstructed over some area surrounding a vessel or structure of interest by fitting a wave model to a large data set of measured surface elevations, acquired for instance with: (i) a X-band radar (Nieto Borge *et al.* 2004; Dankert & Rosenthal 2004; Hilmer & Thornhill 2014; Qi *et al.* 2016; Naaijen *et al.* 2018); or (ii) a LIDAR camera (Belmont *et al.* 2007; Noguier *et al.* 2014). LIDAR cameras operate in the visible light (e.g., green laser of μm wavelength) and make direct (geo-referenced) measurements of the ocean surface; hence, they have the potential to finely sample the ocean surface and thus resolve higher frequency waves. By contrast, X-band radars operate in the micro-wave regime (typically at a ~ 3 cm wavelength) and invert surface elevations by way of a modulation transfer function (MTF), which relates slope modulations of a resonant Bragg wavelength (~ 1.5 cm) to characteristics of longer gravity waves. Although greatly improved in recent years, X-band radars are still limited to resolving gravity waves with wavelengths of a few tens of meter (e.g., 30 m) or longer in the sea state (Hilmer & Thornhill 2014). Both X-band radar and LIDAR data measured by an instrument located on board the considered structure or vessel are acquired at grazing incidence. Hence, measured free surface data both has a geometrically decreasing density with distance and suffers from gaps due to wave shadowing effects. The latter typically do not penalize the inversion of X-band radar data, which uses a ‘shadowing mask’ that in fact benefits the inversion. For LIDAR cameras, shadowing effects can be alleviated by using spatio-temporal data, in the form of high frequency snapshots of measured surface elevations (Noguier *et al.* 2014).

Such a spatio-temporal reconstruction method was proposed by Grilli *et al.* (2011) and Noguier *et al.* (2014) who applied it to synthetic data, of the type that would be acquired by a Flash LIDARTM camera (ASC 2018), which can take high-density (up to 128 by 128 simultaneous measurement points) and high-frequency (about 10 Hz) snapshots of the ocean surface. These authors pointed out that, given enough components (in a Fourier sense), a linear ocean surface reconstruction (‘nowcast’) was always accurate. However, even for moderate nonlinearity, the linear propagation of this surface was increasingly in error as time increased, due to a modified dispersion relation. Hence, a nonlinear wave model should be used, even to issue a short-term forecast (e.g., 15-20 s).

In this realm, since it was first proposed by Dommermuth & Yue (1987) and West *et al.* (1987), the High-Order Spectral (HOS) method has been extensively used for the time-domain simulation of nonlinear irregular sea states, including their reconstruction and propagation on the basis of individual measurements at wave gauges (Ducrozet *et al.* 2007; Bonnefoy *et al.* 2009; Blondel-Couprie *et al.* 2013; Qi *et al.* 2018a). The recent paper by Qi *et al.* (2018a) in fact provides a complete review of such work to date, as well as a discussion of the important aspects of the a priori identification of a relevant space-time prediction zone as a function of the measurement zone Qi *et al.* (2018b). In operational situations, however, even considering the recently increasing performance and compactness of computing hardware (e.g., General Purpose Graphical Processing Units (GPGPU)), the nonlinear inversion required at each time to perform a nonlinear ocean surface reconstruction and propagation with the HOS method may be prohibitive to use in real time.

For issuing real-time predictions based on a set of surface measurements, it is thus desirable to perform both the reconstruction and propagation of nonlinear ocean surfaces using a more efficient nonlinear wave model. An interesting approach to simulate

nonlinear wave properties at lower computational cost is to use Lagrangian wave models (see, e.g., Clamond (2007) for a detailed overview). Gerstner (1809) developed a first-order two-dimensional (2D) Lagrangian model for periodic ocean waves, referred to as ‘trochoidal wave theory’, and showed that his model could predict higher-order wave properties (in terms of wave steepness $\epsilon = ak$, with $a = H/2$ the wave amplitude, $k = 2\pi/\lambda$ the wavenumber, and λ the wavelength) such as surface slope, at a lower-order of development. [Note that Gerstner’s theory is rotational, but this is irrelevant here since we are only concerned by the ocean surface geometry.] Besides this interesting property, Lagrangian models take the form of a computationally efficient explicit time stepping scheme, in which surface elevations at the next time level are easily predicted based on current time. The advantage of using Lagrangian wave models to more realistically simulate irregular waves in severe sea states, and in particular wave asymmetry, was first noted by Lindgren & Åberg (2009) (see also Lindgren (2009, 2010, 2015)). To efficiently propagate nonlinear and irregular ocean surfaces in space and time, Noguier *et al.* (2009) developed the ‘Choppy Wave Model’ (CWM), which extended Gerstner’s theory to three-dimensional (3D) non-periodic waves, and showed that it correctly approximates second-order wave properties for narrow-banded spectra, such as asymmetry in wave elevation and surface slope. To further improve nonlinear wave properties Noguier *et al.* (2015) developed a complete second-order Lagrangian wave model, as an extension of CWM, referred to hereafter as CWM2; they showed that this model correctly accounted for third-order wave properties, but with a much increased computational cost as compared to CWM.

Grilli *et al.* (2011) and Noguier *et al.* (2014) applied the CWM to simulated LIDAR data and showed that it could accurately reconstruct and propagate nonlinear sea-states of moderate steepness for a short time (a few peak spectral periods T_p). For larger times or wave steepness, however, our recent numerical comparisons with a third-order reference HOS solution show that errors increase to unacceptable levels during propagation. Increasing phase shifts in the reconstructed sea state were identified as the main reasons for these large errors, which resulted from errors in wave phase velocity. Indeed, at Lagrangian first-order, or Eulerian second-order, phase velocity is identical to the linear celerity, $c_0 = \omega/k = g/\omega$ (in deep water, with g the gravitational acceleration, k the wavenumber, and ω the wave angular frequency).

In this paper, considering we are mainly concerned with an accurate geometrical description of nonlinear ocean surfaces, as well as their propagation, we propose an improvement to the CWM that adequately corrects for this nonlinear wave celerity error by adding a ‘Stokes drift’ term to the linear celerity. Our proposed theoretical approach allows to obtain, from standard second-order Eulerian results and with few additional calculations, the second-order Lagrangian expansion of particle locations on the ocean surface; such results were already derived from first principles by several authors, albeit through very complex calculations (Pierson (1961, 1962); Noguier *et al.* (2015)). By following the trajectory of such particles, the free surface geometry can easily be reconstructed. The key aspect of our approach is that it provides a higher-order of approximation of the free surface than the second-order Eulerian expansion, as it features some higher-order Eulerian components (Noguier *et al.* 2015). We combine this simplified Lagrangian approach with an improved choice of the reference particle location, which makes it possible to correct some discrepancies with the nonlinear wave dispersion relationship.

We first develop and validate this improved model in 2D, hereafter referred to as ‘Improved Choppy Wave Model’ (ICWM). For periodic waves we show that it is fully consistent with the nonlinear time evolution at Eulerian third-order; for irregular waves

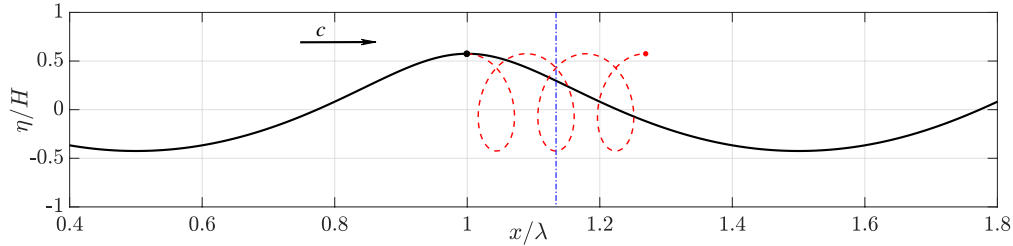


FIGURE 1. Sketch illustrating the Lagrangian trajectory (red dashed line) of a water particle initially located at (x_0, z_0) (●), on the free surface of a 2D (long-crested) nonlinear periodic wave (solid line; generated with the second-order ‘Choppy’ wave theory Eqs. (2.3)) of height $H = 2a$, wavelength λ , steepness $\epsilon = ka = 0.3$, and propagating left-to-right with celerity $c = \omega/k$ (with $k = 2\pi/\lambda$ the wavenumber; in deep water, if $a = 3$ m, the wave period $T = 2\pi/\omega = 6.35$ s). After $t = 3T$, the particle has moved forward by $\mathcal{U}_{s0}t$ (●) and its mean horizontal location during this motion is $\mathcal{U}_{s0}t/2$ (blue chained line). Consistent with Choppy wave theory, the mean water level (MWL) has been shifted upwards by $\epsilon a/2$.

we show that it brings a significant improvement in the non-linear time evolution while having the same computational complexity as the CWM. We show that, as time increases, the second-order CWM2 Lagrangian interaction terms which are discarded in the ICWM become increasingly negligible for propagating irregular waves. We perform validation tests for both narrow- and broad-banded spectra and compare errors of the linear, CWM, CWM2 and ICWM models with respect to a fully nonlinear HOS model solution. We also present the CWM2 analytical extension to 3D in the Appendix, although numerical applications and validations of the latter will be left out for future work.

In the following, in Section 2, we first discuss an apparent paradox that leads to different expressions of the third-order Lagrangian and Eulerian wave celerities. This paradox is resolved in Section 3 for 2D periodic waves, leading to corrected Lagrangian evolution equations used in the ICWM. Section 4 generalizes this formulation to 2D irregular waves; its relevance and accuracy are numerically assessed in Section 5 by considering two generic wave spectra. The case of 3D irregular waves is left in the Appendix for conciseness of the core of the paper.

2. An apparent Stokes drift paradox

Nonlinear ocean waves induce a time-averaged mass transport velocity in their direction of propagation, referred to as Stokes drift and hereafter denoted in deep water by $\mathcal{U}_s = \mathcal{U}_{s0} \exp(2kz)$ (Fig. 1), where \mathcal{U}_{s0} denotes the Stokes drift on the free surface. For two-dimensional (2D) (i.e., long-crested) periodic waves, \mathcal{U}_s can be computed by time-averaging over the wave period $T = 2\pi/\omega$ (or space-averaging over the wavelength) either the horizontal Eulerian velocity $U(x, z, t)$ at a fixed x location, or the Lagrangian velocity $U(X(t), Z(t), t)$, following the trajectory $(X(t), Z(t))$ of a water particle of initial location (x_0, z_0) . Both results should be identical (see Clamond (2007) for a detailed discussion). The mean Lagrangian mass transport velocity \bar{U}_L can then be calculated as the depth-averaged of the Stokes drift \mathcal{U}_s , which will be less than \mathcal{U}_{s0} (Monismith *et al.* 2007).

Pierson (1961, 1962) and Noguier *et al.* (2009, 2015) derived Lagrangian equations for deep-water periodic waves, as a perturbation expansion in order of wave steepness ϵ .

To second-order they found the trajectories of a particle of initial location (x_0, z_0) as:

$$\begin{aligned} X(t) &= x_0 - a \sin(kx_0 - \omega t)e^{kz_0} + \mathcal{U}_{s0} e^{2kz_0} t, \\ Z(t) &= z_0 + \frac{1}{2}ka^2 + a \cos(kx_0 - \omega t)e^{kz_0} \end{aligned} \quad (2.1)$$

with $\omega^2 = gk$, the deep water dispersion relationship,

$$\mathcal{U}_{s0} = ka^2\omega = \epsilon^2 c_0 \quad (2.2)$$

and $c_0 = \omega/k = \sqrt{g/k}$ the linear deep water phase velocity (or celerity). In Eq. (2.1), the zeroth-order solution is the particle at rest at its initial location (x_0, z_0) , the first-order solution is the classical Gerstner (1809) trochoidal wave theory, and the second-order correction is limited to the effect of the Stokes drift over time t , $\mathcal{U}_s t$.

The corresponding free surface geometry is implicitly described by the trajectories of particles located on the mean water level (MWL), at $z_0 = 0$ (Fig. 1):

$$\begin{aligned} X(t) &= x_0 - a \sin(kx_0 - \omega t) + \mathcal{U}_{s0} t, \\ Z(t) &= \frac{1}{2}ka^2 + a \cos(kx_0 - \omega t) \end{aligned} \quad (2.3)$$

Due to Stokes drift, these are ‘open’ trajectories, i.e., after each wave period, water particles do not travel back to their initial location, but instead have a forward horizontal displacement $\mathcal{U}_{s0}T$ on the free surface. Clamond (2007) shows (his Fig. 1) that when corrected by this mass transport the particle trajectories describe closed trajectories.

After some simple algebra, an explicit relationship, $Z(t) = \eta_L(X(t), t)$ can be iteratively obtained, which yields:

$$k\eta_L(x, t) = \left(\epsilon - \frac{3}{8}\epsilon^3\right) \cos k(x - c_L t) + \frac{1}{2}\epsilon^2 \cos 2k(x - c_L t) + \frac{3}{8}\epsilon^3 \cos 3k(x - c_L t) + \mathcal{O}(\epsilon^4), \quad (2.4)$$

with the modified dispersion relationship:

$$c_L = c_0(1 + \epsilon^2) \quad (2.5)$$

At $t = 0$, Eq. (2.4) is fully consistent[†] with a third-order Stokes expansion. This is expected from Lagrangian wave equations, which typically provide an order of approximation higher by one as compared to the corresponding Eulerian equations. However, the nonlinear Lagrangian dispersion relationship Eq. (2.5) found here is different from the third-order Eulerian solution (e.g., Fenton (1985)):

$$c_E = c_0\left(1 + \frac{1}{2}\epsilon^2\right) \quad (2.6)$$

Thus, the correction to the linear wave celerity predicted by the Lagrangian solution at second-order is twice the correction predicted by the third-order Eulerian solution. This discrepancy was already noted by Pierson (1961), but he could not resolve the contradiction and only stated that “there probably is a residual vorticity field at third-order in the Lagrangian solution that may account for the difference”. As we will show, it turns out that the vorticity is not the reason for this discrepancy, which is only apparent and results from the choice made of the reference location of the Lagrangian particles as time increases.

[†] This was already noted by Noguier *et al.* (2009) in equation (63) but with a misprint in the sign of the $\cos 2kx$ factor.

3. Corrected Lagrangian evolution equations for periodic waves

3.1. Choice of reference particle location

To ensure that a Lagrangian perturbation expansion in order of steepness, such as Eq. (2.3), converges, particles must undertake “small” displacements with respect to their reference location. Hence, using the zeroth-order solution (x_0, z_0) as a particle reference location is increasingly in error, as the secular term $\mathcal{U}_s t$ due to Stokes drift eventually transports particles far away from their initial location.

More specifically, as the focus of this study is the free surface geometry and kinematics, let us consider the trajectory of a free surface particle in a periodic wave over one periods T . The horizontal position of the particle has shifted with respect to its initial location by, $X(T) - X(0) = \mathcal{U}_{s0} T$, i.e., proportionally to the free surface value of the Stokes drift. However, based on Eq. (2.3), the mean horizontal location of the particle:

$$\frac{1}{T} \int_0^T X(t) dt = x_0 + \frac{1}{2} \mathcal{U}_{s0} T, \quad (3.1)$$

has only moved horizontally by half this distance. Hence, the barycenter of the trajectory propagates at only half the speed of the free surface Stokes drift. Therefore, the maximum excursion of the particle location with respect to its barycenter is on the order of $\frac{1}{2} \mathcal{U}_{s0} T$, while the maximum excursion of the particle with respect to its location at rest is twice as much. This result implies that the initial particle position is not an appropriate choice of a reference location. As we will see in the following section, to accurately simulate the Eulerian phase velocity at third-order, the Lagrangian evolution equations should be revised by performing a perturbation expansion about a moving reference location at a translation speed which will be optimized.

3.2. A simple derivation of the Lagrangian solution

For a periodic wave, rather than solving the complete dynamical Lagrangian equations as was done in Pierson (1961) and Noguier *et al.* (2015), a simple Lagrangian solution can be derived for the particle motion based on the standard Eulerian velocity field $(U(x, z, t), W(x, z, t))$, by solving:

$$\begin{aligned} \dot{X}(t) &= U(X(t), Z(t), t) \\ \dot{Z}(t) &= W(X(t), Z(t), t) \end{aligned} \quad (3.2)$$

where the dot superscripts denote time derivatives. Following the standard procedure, we describe the particle location by its fluctuations with respect to its resting location, (x_0, z_0) ,

$$\begin{aligned} X(t) &= x_0 + x(t), \\ Z(t) &= z_0 + z(t). \end{aligned} \quad (3.3)$$

Assuming small fluctuations, we may then perform a first-order Taylor series expansion of the Eulerian velocity around the resting location, which yields:

$$\begin{aligned} \dot{X}(t) = \dot{x}(t) &= U(x_0, z_0, t) + x(t) \frac{\partial U}{\partial x}(x_0, z_0, t) + z(t) \frac{\partial U}{\partial z}(x_0, z_0, t) + \mathcal{R}_x, \\ \dot{Z}(t) = \dot{z}(t) &= W(x_0, z_0, t) + x(t) \frac{\partial W}{\partial x}(x_0, z_0, t) + z(t) \frac{\partial W}{\partial z}(x_0, z_0, t) + \mathcal{R}_z, \end{aligned} \quad (3.4)$$

where $\mathcal{R}_x, \mathcal{R}_z$ denote truncation errors, which will be quantified later. The second-order Eulerian velocity field in deep water reads (e.g., Dean & Dalrymple (1991)):

$$\begin{aligned} kU(x, z, t) &= \epsilon\omega e^{kz} \cos(kx - \omega t) + \mathcal{O}(\epsilon^3) = kU_1 + \mathcal{O}(\epsilon^3) \\ kW(x, z, t) &= \epsilon\omega e^{kz} \sin(kx - \omega t) + \mathcal{O}(\epsilon^3) = kW_1 + \mathcal{O}(\epsilon^3). \end{aligned} \quad (3.5)$$

Note that the dominant terms are first-order in steepness and the next terms are non-zero only at third-order. Anticipating that the dimensionless fluctuations ($kx(t), kz(t)$) are also of first-order in steepness, it follows that the products in Eq. (3.4) are of $\mathcal{O}(\epsilon^2)$ and the errors \mathcal{R}_x and \mathcal{R}_z are of $\mathcal{O}(\epsilon^3)$. Hence, the first-order contributions to the particle motion satisfy:

$$\begin{aligned} k \overset{\circ}{x}_1(t) &= \epsilon\omega e^{kz_0} \cos(kx_0 - \omega t) \\ k \overset{\circ}{z}_1(t) &= \epsilon\omega e^{kz_0} \sin(kx_0 - \omega t) \end{aligned} \quad (3.6)$$

which yields,

$$\begin{aligned} x_1(t) &= -ae^{kz_0} \sin(kx_0 - \omega t) \\ z_1(t) &= ae^{kz_0} \cos(kx_0 - \omega t). \end{aligned} \quad (3.7)$$

The governing equation for the next order in particle motion (x_2, z_2) is found by inserting Eq. (3.7) into Eq. (3.4) and retaining the second-order terms in steepness:

$$\begin{aligned} \overset{\circ}{x}_2(t) &= U_2(x_0, z_0, t) + x_1(t) \frac{\partial U_1}{\partial x}(x_0, z_0, t) + z_1(t) \frac{\partial U_1}{\partial z}(x_0, z_0, t) \\ \overset{\circ}{z}_2(t) &= W_2(x_0, z_0, t) + x_1(t) \frac{\partial W_1}{\partial x}(x_0, z_0, t) + z_1(t) \frac{\partial W_1}{\partial z}(x_0, z_0, t) \end{aligned} \quad (3.8)$$

Since, in deep water $U_2 = W_2 = 0$, as seen in Eq. (3.5), this equation simplifies to:

$$\begin{aligned} \overset{\circ}{x}_2(t) &= \mathcal{U}_{s0} e^{2kz_0} \\ \overset{\circ}{z}_2(t) &= 0, \end{aligned} \quad (3.9)$$

whose solution is:

$$\begin{aligned} x_2(t) &= \mathcal{U}_{s0} e^{2kz_0} t \\ z_2(t) &= 0, \end{aligned} \quad (3.10)$$

Note that, assuming that the initial particle trajectory (at $t = 0$) is centered about its resting location (x_0, z_0), the integration constants in Eqs. (3.7) and (3.10) were set to zero. Summarizing our results so far we have:

$$\begin{aligned} kX(t) &= kx_0 - \epsilon \sin(kx_0 - \omega t) e^{kz_0} + k\mathcal{U}_{s0} e^{2kz_0} t + \mathcal{O}(\epsilon^3) \\ kZ(t) &= kz_0 + \epsilon \cos(kx_0 - \omega t) e^{kz_0} + \mathcal{O}(\epsilon^3) \end{aligned} \quad (3.11)$$

Now in view of the secular term $k\mathcal{U}_{s0} e^{2kz_0} t$, the horizontal fluctuation will become arbitrarily large as time increases and cause the perturbation expansion to break down. The magnitude of the horizontal particle fluctuation over a given time interval $[0, t]$ can be quantified by the mean square distance to the reference location:

$$\langle x^2 \rangle_t = \frac{1}{t} \int_0^t x^2(t') dt' \quad (3.12)$$

For a large number n of completed cycles we find (with $(n-1)T \leq t < nT$):

$$\langle x^2 \rangle_t \simeq \langle x^2 \rangle_{nT} \simeq \frac{1}{3} (nT)^2 \mathcal{U}_{s0}^2 e^{4kz_0}, \quad (3.13)$$

where we have neglected the bounded terms. Based on this equation, the choice of the initial resting location of the particle (x_0, z_0) as a reference location is clearly not optimal since the particle increasingly drifts away from it with each passing cycle. Hence we propose to correct this reference location in order to minimize the influence of the secular term in the horizontal motion of the particle. To do so, the perturbation expansion Eq. (3.3) is recast using a reference location (\bar{x}, \bar{z}) as a linear function of the Stokes drift that takes place over the time interval under consideration, i.e., $\bar{x} = x_0 + \alpha \mathcal{U}_{s0} e^{2kz_0} nT$. Proceeding with calculations in a way similar to Eqs. (3.4-3.11), we obtain the expression of the second-order fluctuation $(x(t), z(t))$ with respect to this new reference position, which is valid for all time in the interval $[0, nT]$:

$$\begin{aligned} kX(t) &= k(\bar{x} + x(t)) = k\bar{x} - \epsilon \sin(k\bar{x} - \omega t) e^{k\bar{z}} + k\mathcal{U}_{s0} (t - \alpha nT) e^{2k\bar{z}} + \mathcal{O}(\epsilon^3) \\ kZ(t) &= k(\bar{z} + z(t)) = k\bar{z} + \epsilon \cos(k\bar{x} - \omega t) e^{k\bar{z}} + \mathcal{O}(\epsilon^3), \end{aligned} \quad (3.14)$$

where the integration constant $-\alpha nT$ in the secular term ensures the consistency at $t = 0$ with the original expansion Eq. (3.11). The optimal value of α can now be selected such as to minimize the mean square fluctuation $\langle x^2 \rangle_{nT}$, which yields $\alpha = \frac{1}{2}$ and:

$$\langle x^2 \rangle_{nT} \simeq \frac{1}{12} (nT)^2 \mathcal{U}_{s0}^2 e^{4kz_0} \quad (3.15)$$

With this parametrization, the horizontal reference location is finally found to be the average particle motion over the completed cycles:

$$\bar{x} = x_0 + \frac{1}{2} \mathcal{U}_{s0} e^{2kz_0} nT = \frac{1}{nT} \int_0^{nT} X(t) dt \quad (3.16)$$

Note that, with the induced correction, the reference location is recalculated at each new cycle of particle motion, that is $(n-1)T \leq t < nT$ in eq. (3.16) above. For the reference vertical location, we select:

$$\bar{z}_0 = z_0 + \frac{1}{2} k^{-1} \epsilon^2 \quad (3.17)$$

which ensures that the corresponding Eulerian surface is vertically centered, as can be seen from Eqs. (2.3) and (2.4).

For the free surface particles ($z_0 = 0$), which are those of interest in this work, this finally yields:

$$\begin{aligned} kX(t) &= kx_0 - \epsilon \sin(kx_0 + \frac{1}{2} k\mathcal{U}_{s0} nT - \omega t) + k\mathcal{U}_{s0} t + \mathcal{O}(\epsilon^3) \\ kZ(t) &= \frac{1}{2} \epsilon^2 + \epsilon \cos(kx_0 + \frac{1}{2} k\mathcal{U}_{s0} nT - \omega t) + \mathcal{O}(\epsilon^3), \end{aligned} \quad (3.18)$$

Since $k\mathcal{U}_{s0} |t - nT| \leq kT\mathcal{U}_{s0} = \mathcal{O}(\epsilon^2)$, Eq. (3.18) can be recast in a simpler way, within a third-order truncation error:

$$\begin{aligned} kX(t) &= kx_0 - \epsilon \sin(kx_0 - \tilde{\omega} t) + k\mathcal{U}_{s0} t \\ kZ(t) &= \frac{1}{2} \epsilon^2 + \epsilon \cos(kx_0 - \tilde{\omega} t) \end{aligned} \quad (3.19)$$

for any time $t \geq 0$, in which the modified angular frequency is defined as:

$$\tilde{\omega} = \omega - \frac{1}{2} k\mathcal{U}_{s0}. \quad (3.20)$$

This equation, which is consistent with the original Choppy wave model at $t = 0$, yields

the correct value of the Stokes drift on the free surface:

$$\frac{1}{t} \int_0^t \overset{\circ}{X}(t') dt' = \mathcal{U}_{s0} \quad (3.21)$$

and is consistent with the third-order Stokes wave dispersion relationship Eq. (2.6), as seen by comparing it with Eqs. (2.3)-(2.4).

As seen above the proposed correction of a “moving” horizontal reference location \bar{x}_n leads to a modified dispersion relationship, which is in fact simply related to the “speed” of any reference particle. It can indeed be easily checked, by performing calculations similar to above, that selecting a reference particle on the free surface that translates at a fraction α of the Stokes drift, that is $\bar{x}_n = x_0 + n\alpha\mathcal{U}_{s0}T$ leads to a propagation speed $c_L = c_0(1 + (1 - \alpha)\epsilon^2)$. The selected value $\alpha = \frac{1}{2}$ yields results consistent with the nonlinear dispersion relationship predicted by third-order Eulerian theory. However, this value was not found by requiring a priori compliance to the latter, but through a more general optimization criterion, ensuring that the mean square fluctuation of horizontal particle motions along their trajectory be minimal. When considering Eq. (3.14), the perturbation expansion could appear to be an artificial redistribution of the second-order terms in $O(\epsilon^2)$, between the secular term and the moving reference location. However, the difference is hidden in the $O(\epsilon^3)$ term, which can also grow arbitrarily due to any combination of the form $x_2 \frac{\partial U_1}{\partial x}$ or $x_2 \frac{\partial W_1}{\partial x}$ in the dynamical Lagrangian Eq. (3.2).

4. Generalization to two-dimensional irregular waves

4.1. Derivation of the Lagrangian solution

The case of irregular waves can be derived in a similar way. We again seek to express the particle locations $(X(t), Z(t))$ as a perturbation expansion around some reference location (\bar{x}, \bar{z}) :

$$\begin{aligned} X(t) &= \bar{x} + x_1(t) + x_2(t), \\ Z(t) &= \bar{z} + z_1(t) + z_2(t) \end{aligned} \quad (4.1)$$

up to second-order in total wave steepness ϵ , where again the mean location (\bar{x}, \bar{z}) does not necessarily coincide with the particle resting location (x_0, z_0) .

Assuming a 2D sea state represented by an energy density spectrum $S(\omega)$, of peak spectral period $T_p = 2\pi/\omega_p$, linear irregular wave elevations can be defined in deep water as the superposition of periodic components (or harmonics) of increasing angular frequencies ω_i ($i = 1, \dots, N$) separated by a frequency step $\Delta\omega$:

$$\eta_1(x, t) = \sum_{i=1}^N a_i \cos \psi_i, \quad (4.2)$$

of amplitudes $a_i = \sqrt{2S(\omega_i)\Delta\omega}$ and phase functions $\psi_i = k_i x - \omega_i t - \varphi_i$, with $k_i = \omega_i^2/g$ and $\varphi_i \in [0, 2\pi]$ the component wavenumbers and random phases, respectively. For this wave field, the total steepness is defined as $\epsilon = \sum_i a_i k_i$ and, according to standard spectral wave theory, the sea state’s significant wave height is defined as $H_s = 4\sqrt{m_o}$, where $m_o = \int_0^\infty S(\omega) d\omega \simeq \Delta\omega \sum_i S_i$ is the zeroth-moment or area of the spectrum.

The linear velocity field corresponding to Eq. (4.2) is given by:

$$\begin{aligned} U^{(1)}(x, z, t) &= \sum_{i=1}^N a_i \omega_i e^{k_i z} \cos \psi_i \\ W^{(1)}(x, z, t) &= \sum_{i=1}^N a_i \omega_i e^{k_i z} \sin \psi_i \end{aligned} \quad (4.3)$$

For irregular waves, however, unlike the periodic wave case of Eq. (3.5), second-order terms ($U^{(2)}, W^{(2)}$) appear in the velocity field, whose expressions were derived by Longuet-Higgins (1963) (based on the velocity potential given on p 466). Assuming long-crested waves, the second-order velocity potential reads:

$$\phi^{(2)}(x, z, t) = \sum_{i,j} 2a_i a_j \omega_i \omega_j \frac{(\omega_i - \omega_j)}{(\omega_i - \omega_j)^2 - g |k_i - k_j|} e^{|k_i - k_j| z} \sin(\psi_i - \psi_j), \quad (4.4)$$

which after some algebra can be recast more simply as:

$$\phi^{(2)}(x, z, t) = - \sum_{i < j} a_i a_j \omega_j e^{(k_j - k_i) z} \sin(\psi_j - \psi_i), \quad (4.5)$$

leading to:

$$\begin{aligned} U^{(2)}(x, z, t) &= \frac{\partial \phi^{(2)}}{\partial x}(x, z, t) = - \sum_{i < j} a_i a_j \omega_j \frac{(\omega_j^2 - \omega_i^2)}{g} e^{(k_j - k_i) z} \cos(\psi_j - \psi_i) \\ W^{(2)}(x, z, t) &= \frac{\partial \phi^{(2)}}{\partial z}(x, z, t) = - \sum_{i < j} a_i a_j \omega_j \frac{(\omega_j^2 - \omega_i^2)}{g} e^{(k_j - k_i) z} \sin(\psi_j - \psi_i) \end{aligned} \quad (4.6)$$

Following the procedure used for periodic waves, we perform a Taylor series expansion of the velocity field around the reference location of the considered particle (\bar{x}, \bar{z}) (to be defined later) and eliminate third-order and higher-order terms in steepness, which yields:

$$\begin{aligned} \overset{\circ}{x}(t) &= U^{(1)}(\bar{x}, \bar{z}, t) + U^{(2)}(\bar{x}, \bar{z}, t) + x(t) \frac{\partial U^{(1)}}{\partial x}(\bar{x}, \bar{z}, t) + z(t) \frac{\partial U^{(1)}}{\partial z}(\bar{x}, \bar{z}, t) + \mathcal{O}(\epsilon^3) \\ \overset{\circ}{z}(t) &= W^{(1)}(\bar{x}, \bar{z}, t) + W^{(2)}(\bar{x}, \bar{z}, t) + x(t) \frac{\partial W^{(1)}}{\partial x}(\bar{x}, \bar{z}, t) + z(t) \frac{\partial W^{(1)}}{\partial z}(\bar{x}, \bar{z}, t) + \mathcal{O}(\epsilon^3) \end{aligned} \quad (4.7)$$

Inserting the expressions of $U^{(1)}$ and $W^{(1)}$ in this set of equations yields the first-order time derivatives of the particles locations as:

$$\begin{aligned} \overset{\circ}{x}_1(t) &= \sum_{i=1}^N a_i \omega_i e^{k_i \bar{z}} \cos \bar{\psi}_i, \\ \overset{\circ}{z}_1(t) &= \sum_{i=1}^N a_i \omega_i e^{k_i \bar{z}} \sin \bar{\psi}_i \end{aligned} \quad (4.8)$$

where $\bar{\psi}_i = k_i \bar{x} - \omega_i t - \varphi_i$. The integration of the first-order particle trajectories is

straightforward:

$$\begin{aligned} x_1(t) &= -\sum_{i=1}^N a_i e^{k_i \bar{z}} \sin \bar{\psi}_i, \\ z_1(t) &= \sum_{i=1}^N a_i e^{k_i \bar{z}} \cos \bar{\psi}_i, \end{aligned} \quad (4.9)$$

with zero integration constants as these quantities are already of zero average. Next, inserting the expressions of $U^{(2)}$, $W^{(2)}$ from Eq. (4.6) and Eq. (4.9) into Eq. (4.7) yields:

$$\begin{aligned} \overset{\circ}{x}_2(t) &= \sum_{i<j} \frac{a_i a_j}{g} \cos \bar{\psi}_{ij} \left[-\omega_j (\omega_j^2 - \omega_i^2) e^{(k_j - k_i) \bar{z}} + (\omega_j^3 + \omega_i^3) e^{(k_j + k_i) \bar{z}} \right] + \sum_{i=1}^N a_i^2 k_i \omega_i e^{2k_i \bar{z}} \\ \overset{\circ}{z}_2(t) &= \sum_{i<j} \frac{a_i a_j}{g} \sin \bar{\psi}_{ij} \left[-\omega_j (\omega_j^2 - \omega_i^2) e^{(k_j - k_i) \bar{z}} + (\omega_j^3 - \omega_i^3) e^{(k_j + k_i) \bar{z}} \right] \end{aligned} \quad (4.10)$$

where $\bar{\psi}_{ij} = \bar{\psi}_j - \bar{\psi}_i$.

The integration of the time derivatives of the second-order terms must be done more carefully, as it leads to singular expressions. When integrating from some initial time, say $t = 0$, we find:

$$\begin{aligned} x_2(t) &= \sum_{i<j} \frac{a_i a_j}{g} \left(\omega_j (\omega_j + \omega_i) e^{(k_j - k_i) \bar{z}} - \frac{(\omega_j^3 + \omega_i^3)}{(\omega_j - \omega_i)} e^{(k_j + k_i) \bar{z}} \right) (\sin \bar{\psi}_{ij} - \sin \bar{\psi}_{ij}|_{t=0}) \\ &\quad + \sum_{i=1}^N a_i^2 k_i \omega_i e^{2k_i \bar{z}} t + C_x \\ z_2(t) &= \sum_{i<j} \frac{a_i a_j}{g} \left(-\omega_j (\omega_j + \omega_i) e^{(k_j - k_i) \bar{z}} + \frac{(\omega_j^3 - \omega_i^3)}{(\omega_j - \omega_i)} e^{(k_j + k_i) \bar{z}} \right) \cos \bar{\psi}_{ij} + C_z, \end{aligned} \quad (4.11)$$

within some integration constants (C_x, C_z). Note that the difference of sine terms in the summation for $x_2(t)$ balances the $1/(\omega_j - \omega_i)$ singularity in the kernel, which would otherwise lead to a divergent summation with a decreasing frequency step.

4.2. The second-order 'Choppy Wave Model'

When the reference particle location is selected as that of the surface at rest, ($\bar{x} = x_0, \bar{z} = z_0$), Eq. (4.9) recovers the first-order Lagrangian solution of Pierson (1961). When applied to the free surface particles ($z_0 = 0$), this recovers the 'Choppy Wave Model' (CWM) Noguier *et al.* (2009). For the same choice of reference particle location and setting $C_x = C_z = 0$, Eqs. (4.9) and (4.11) coincide with the second-order expressions derived by Pierson (1961) for $x_2(t) - x_2(0)$. Finally, with $C_x = 0$ and $C_z = \frac{1}{2} \sum_{i=1}^N a_i^2 k_i$ the equations coincide with the expansion derived by Noguier *et al.* (2015) for the same quantity. By analogy with the first-order case, this latter version of the second-order expansion specified on the free surface ($z_0 = 0$) will be referred to as 'second-order Choppy Wave Model', abbreviated to 'CWM2' in the following.

After some algebraic simplifications that occur for $z_0 = 0$ and using the linear disper-

sion relationship, the complete CWM2 expansion reads:

$$\begin{aligned} X(t) &= x_0 - \sum_{i=1}^N a_i \sin \psi_i^0 + \sum_{i<j} a_i a_j B_{ij}^x (\sin \psi_{ij}^0 - \sin \psi_{ij}^0|_{t=0}) + \mathcal{U}_{s0} t \\ Z(t) &= \frac{1}{2} \sum_{i=1}^N a_i^2 k_i + \sum_{i=1}^N a_i \cos \psi_i^0 + \sum_{i<j} a_i a_j B_{ij}^z \cos \psi_{ij}^0, \end{aligned} \quad (4.12)$$

where $\psi_i^0 = k_i x_0 - \omega_i t - \varphi_i$ and $\psi_{ij}^0 = \psi_j^0 - \psi_i^0$. Here \mathcal{U}_{s0} is the total Stokes drift of the irregular wave field on the free surface, defined as:

$$\mathcal{U}_{s0} = \sum_{i=1}^N a_i^2 k_i \omega_i \quad (4.13)$$

and,

$$\begin{aligned} B_{ij}^x &= k_i \frac{\omega_i + \omega_j}{\omega_i - \omega_j} \\ B_{ij}^z &= k_i. \end{aligned} \quad (4.14)$$

As compared to the CWM1, the CWM2 includes wave interaction terms for both the horizontal and vertical position, represented by the double summations in Eq. (4.12). As was shown in Noguier *et al.* (2015), only the wave interaction terms in $Z(t)$ are necessary to make this solution fully consistent with the second-order Eulerian expansion, while the wave interaction terms in $X(t)$ contributes only to third- and higher-order Eulerian expansion and, furthermore, are found numerically unstable. These double summations do not allow for an efficient numerical implementation of the CWM2 model as they require $O(N_x \times N)$ computations at every time step, where N_x is the number of particle positions (corresponding to the grid of surface particles at rest) and N the number of wave frequencies. On the contrary, the CWM1 model can be solved (Noguier *et al.* 2009) by a mere Fast Fourier Transform (FFT) which reduces the computational cost at every time step to $O(N \log N)$. However, it will be shown later that the wave interaction terms have a negligible impact on the performance of the model for predicting the wave evolution in time. Hence, a numerically efficient version of the CWM2 model will be obtained by neglecting these interaction terms (that is keeping in the second-order terms only the Stokes drift and the mean vertical level correction).

4.3. The improved 'Choppy Wave Model'

As in the periodic wave case, the reference particle location (\bar{x}, \bar{z}) will be optimized by requiring that it correspond to the mean particle location over a growing number of cycles. For irregular waves, the free surface is aperiodic but, for a sufficiently long time $t_{max} = nT_p \gg T_p$ (with n a large integer number), it can be assumed that the harmonics in Eqs. (4.9) and (4.11) nearly have a zero average. Hence, calculating the mean particle location to second-order over the time interval $[0, t_{max}]$ and requiring that it be zero yields the Eq. (4.11) constants:

$$\begin{aligned} C_x &= -\frac{1}{2} n \sum_{i=1}^N a_i^2 k_i \omega_i e^{2k_i \bar{z}} T_p \\ C_z &= 0 \end{aligned} \quad (4.15)$$

Note that the integration constant C_x must be updated as the number of peak periods increases. As in the periodic wave case the free surface ($z_0 = 0$) reference particle location

is optimized after n peak periods (\bar{x}_n, \bar{z}_n) by requiring that the MSL of the Lagrangian surface η_L be zero. As we will see, this implies:

$$\bar{z}_n = \bar{z} = \frac{1}{2} \sum_{i=1}^N a_i^2 k_i, \quad (4.16)$$

which is similar to Eq. (3.17) for regular waves.

Next the locus of surface particles (obtained with Eq. (4.16)) is derived, which implicitly defines an Eulerian surface $Z(t) = \eta_L(X(t))$. Based on Eq. (4.9), the first-order displacement with respect to the reference position (\bar{x}, \bar{z}) reads:

$$\begin{aligned} x_1(t) &= - \sum_{i=1}^N a_i \sin \bar{\psi}_i = -D_1(\bar{x}, t) \\ z_1(t) &= \sum_{i=1}^N a_i \cos \bar{\psi}_i = \eta_1(\bar{x}, t), \end{aligned} \quad (4.17)$$

where η_1 is the linear surface elevation from Eq. (4.2) and D_1 is its Hilbert Transform. At second-order, Eq. (4.11) combined with Eq. (4.15) yields:

$$\begin{aligned} x_2(t) &= \sum_{i<j} a_i a_j B_{ij}^x (\sin \bar{\psi}_{ij} - \sin \bar{\psi}_{ij}|_{t=0}) + \mathcal{U}_{s0} (t - \frac{1}{2} n T_p) \\ z_2(t) &= \sum_{i<j} a_i a_j B_{ij}^z \cos \bar{\psi}_{ij}, \end{aligned} \quad (4.18)$$

where the Stokes drift \mathcal{U}_{s0} is defined in Eq. (4.13) and the kernels are given in Eq. (4.14). By comparing the modified second-order expansion (4.18) with the original CWM2, we see that the mean horizontal position \bar{x}_n is related to the position at rest through $x_n = x_0 + \frac{1}{2} n \mathcal{U}_{s0} T_p$. Therefore, for large n , \bar{x} can be replaced by $x_0 + \frac{1}{2} \mathcal{U}_{s0} t$ in Eqs. (4.17) and (4.18), which amounts to replacing $\bar{\psi}_i$ by $\tilde{\psi}_i = k_i x_0 - \tilde{\omega}_i t - \varphi_i$ and $\bar{\psi}_{ij}$ by $\tilde{\psi}_{ij} = \tilde{\psi}_j - \tilde{\psi}_i$ in Eqs. (4.17) and (4.18), with the modified angular frequency:

$$\tilde{\omega}_j = \omega_j - \frac{1}{2} k_j \mathcal{U}_{s0} \quad (4.19)$$

The double summations in the expressions of x_2 and z_2 , in Eqs. (4.17) and (4.18), which represent interaction terms between various harmonics, cannot efficiently be computed (i.e., by a FFT). However, even though their absolute value is on the same order of magnitude as the secular and constant terms in these equations, their fluctuating contributions to the free surface motion average out over a large time and, hence, can be neglected.

Consequently, Eqs. (4.1), (4.17) and (4.18) yield the simplified expressions:

$$\begin{aligned} X(t) &= x_0 - \tilde{D}_1(x_0, t) + \mathcal{U}_{s0} t \\ Z(t) &= \tilde{\eta}_1(x_0, t) + \frac{1}{2} \sum_{i=1}^N a_i^2 k_i, \end{aligned} \quad (4.20)$$

where $\tilde{\eta}_1$ is a linear surface with modified angular frequency and \tilde{D}_1 is its Hilbert Trans-

form:

$$\begin{aligned}\tilde{\eta}_1(x, t) &= \sum_{j=1}^N a_j \cos(k_j x - \tilde{\omega}_j t - \varphi_j), \\ \tilde{D}_1(x, t) &= - \sum_{j=1}^N a_j \sin(k_j x - \tilde{\omega}_j t - \varphi_j)\end{aligned}\quad (4.21)$$

An explicit but approximate formulation of the free surface elevation $Z = \eta_L(X, t)$ can be obtained at second-order by inverting the relationship between X and x_0 and performing a Taylor series expansion in the expression of $Z(t)$:

$$\begin{aligned}x_0 &\simeq X + \tilde{D}_1(X - \mathcal{U}_{s0}t, t) - \mathcal{U}_{s0}t \\ Z(t) &\simeq \tilde{\eta}_1(X - \mathcal{U}_{s0}t, t) + \tilde{D}_1(X - \mathcal{U}_{s0}t, t) \frac{\partial \tilde{\eta}_1}{\partial x}(X - \mathcal{U}_{s0}t, t) + \frac{1}{2} \sum_{i=1}^N a_i^2 k_i\end{aligned}\quad (4.22)$$

Hence, based on Eq. (4.22) the nonlinear surface is defined as:

$$\eta_L(x, t) = \frac{1}{2} \sum_{i=1}^N a_i^2 k_i + \tilde{\eta}_1(x - \mathcal{U}_{s0}t, t) - \tilde{D}_1(x - \mathcal{U}_{s0}t, t) \frac{\partial \tilde{\eta}_1}{\partial x}(X - \mathcal{U}_{s0}t, t) + \dots \quad (4.23)$$

or more explicitly as:

$$\begin{aligned}\eta_L(x, t) &= \frac{1}{2} \sum_{i=1}^N a_i^2 k_i + \sum_{j=1}^N a_j \cos(k_j(x - c_j t) - \varphi_j) \\ &\quad - \sum_{i,j} a_i a_j k_j \sin(k_i(x - c_i t) - \varphi_i) \sin(k_j(x - c_j t) - \varphi_j) + \dots\end{aligned}\quad (4.24)$$

where c_j is the linear phase velocity of each component, c_{0j} , modified by the Stokes drift:

$$c_j = c_{0j} + \frac{1}{2} \mathcal{U}_{s0}, \quad (4.25)$$

with $c_{0j} = \omega_j / k_j$. Note that the resulting free surface is well centered about the horizontal plane ($\langle \eta_L(x, t) \rangle = 0$), which justifies the choice in Eq. (4.16) of the reference vertical value.

The solution (4.19-4.21), hereafter referred to as ICWM, constitutes an improved formulation of the *Choppy Wave* model, which should preserve its high numerical efficiency. Even though second-order interaction terms have been discarded in this model, it retains second-order contributions that are dominant in the time evolution of a wave packet. These are 1) a modified angular frequency (resulting in a modified dispersion relationship); 2) the Stokes drift; and 3) the correction of the mean water level bias (see also Clamond (2007) and his discussion of Gerstner's theory in Appendix). Note that, given spectral amplitudes a_j and initial phases φ_j , a Lagrangian surface $(X(t), Z(t))$ can be efficiently generated with ICWM, at every time step and over a spatial grid x_0 , with the computational cost of 2 FFTs.

5. Assessment of the 2D-ICWM for periodic or irregular waves

The accuracy and efficiency of the proposed improved second-order Lagrangian model (ICWM), to perform the time updating of nonlinear surface waves, are numerically assessed by comparing results to those of a fully nonlinear model based on a High-Order

Spectral method (HOS). In this comparison, we also include the complete original second-order Lagrangian model (CWM2, Eq. (4.12)), where the wave interaction terms in $X(t)$ have been discarded. Finally, for completeness, we also compare results to those of a model based on linear wave theory (LWT).

There are at least three conceptual difficulties when comparing the time evolution of phased-resolved Lagrangian and HOS surfaces, namely:

- (a) the selection of sampling points: Lagrangian and Eulerian surfaces are not evaluated on the same grids;
- (b) non-stationary statistics: because of non-linear interactions, the wave spectrum is evolving in time and thus cannot be prescribed except at initial time;
- (c) the selection of initial phases for an irregular surface: these should be identical in all methods, but cannot in practice be strictly so.

These issues will be further elaborated on below and partial solutions will be implemented in order to achieve a meaningful comparison between the different methods and model results.

5.1. Reference Dataset and Error Definition

A synthetic reference nonlinear ocean surface is first generated using the open source code ‘HOS-ocean’ (Ducrozet *et al.* 2016), which can accurately simulate the propagation of nonlinear waves over large spatio-temporal domains, up to a specified order in wave steepness, albeit at greater computational cost. Since its initial development by Dommermuth & Yue (1987) and West *et al.* (1987), the HOS method has been extensively validated and used in various applications, such as the simulation of freak waves (Ducrozet *et al.* 2007), the implementation of a numerical wave tank (Bonnetoy *et al.* 2009), or ocean wave field reconstructions based on measurements (Blondel-Couprie *et al.* 2013; Qi *et al.* 2018a). HOS-ocean solves the fully nonlinear potential flow problem as a function of time, in terms of N complex amplitudes $A_i(t)$, for many wave components i , which are then used to reconstruct the ocean surface at an arbitrary point (x, t) , as (in 2D):

$$\eta_{\text{HOS}}(x, t) = \text{Re} \left(\sum_{j=1}^N A_j(t) e^{ik_j x} \right). \quad (5.1)$$

In the following applications, we use a fifth-order HOS method with 32 grid points per peak wavelength λ_p , which was verified to provide converged results in terms of order of nonlinearity as well as discretization.

(a) We compare the time evolution of the relative root-mean-square (RMS) difference between the Lagrangian surface η_{LAG} (which can be generated either with CWM2 or ICWM) and the HOS surface elevation η_{HOS} at the same points. Given that the Lagrangian surface is implicitly defined by the surface particle locations, it is much easier to perform this comparison on the Lagrangian grid (that is, the ensemble of points $(X(t), Z(t))$) rather than the Eulerian grid $(x, \eta_{\text{LAG}}(x))$ which requires an explicit formulation of the Lagrangian surface (which can only be attained in an approximate way).

The RMS difference between a free surface representation and the HOS solution is thus defined as:

$$\epsilon_{\text{LAG}}(t) = \frac{1}{\text{rmsh}} \left(\frac{1}{L} \int_0^L \left\{ Z(t) - \eta_{\text{HOS}}(X(t), t) \right\}^2 dX(t) \right)^{1/2} \quad (5.2)$$

where L is the computational domain length and the normalization constant ‘rmsh’ is

defined as:

$$\text{rmsh} = \left(\frac{1}{L} \int_0^L \eta_{\text{HOS}}^2(x, 0) dx \right)^{1/2} = \left(\frac{1}{2} \sum_{i=1}^N |A_i(0)|^2 \right)^{1/2} \quad (5.3)$$

and represents the RMS elevation of the initial surface, which we also express as a function of spectral amplitudes $A_i(0)$.

(b) Given the initial wave spectrum of an irregular surface, the corresponding free surface elevation in the HOS model follows a modified energy density spectrum, due to nonlinear wave-wave interactions and the redistribution of energy that occurs during wave propagation. Hence free surface statistics are not stationary and thus not fully controlled during the nonlinear time evolution. By contrast, CWM surfaces, which are based on a spatial transformation of a linear surface, with a prescribed underlying spectrum, in principle have stationary statistics (that is, their wave spectrum should not evolve in time, even though it can be modified by the bound waves). Hence, a meaningful comparison between time-evolving surfaces in different models can only be performed within smaller time intervals, within which statistics (essentially the energy density spectrum) can be assumed to be stationary. A measure of differences between the initial spectrum and the evolving spectrum of HOS surfaces is given by the RMS difference:

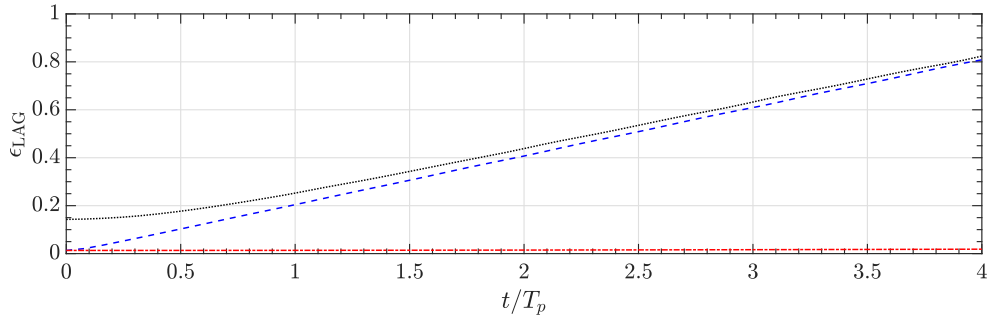
$$\epsilon_{\text{spec}}(t) = \frac{\left(\sum_{i=1}^N (|A_i(t)| - |A_i(0)|)^2 \right)^{1/2}}{\left(\sum_{i=1}^N |A_i(0)|^2 \right)^{1/2}} \quad (5.4)$$

This measure thus provides a lower threshold to the error of Lagrangian methods $\epsilon_{\text{LAG}}(t)$ (defined by Eq. (5.2)), which therefore provides a relevant indicator of the method performance only if, $\epsilon_{\text{spec}}(t) \ll \epsilon_{\text{LAG}}(t)$. In practice, for the typical wave spectra under consideration, we found that this is the case for an evolution time smaller than about 20 to 40 T_p , depending on wave steepness.

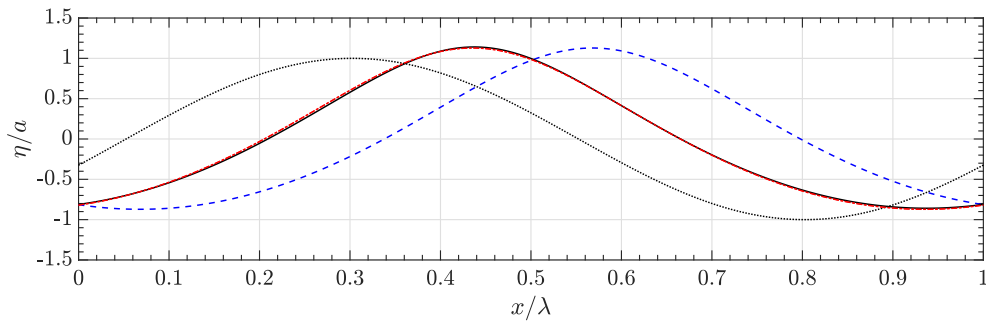
(c) Given an energy density spectrum, phases must be provided for each wave component to generate an initial free surface, which is then propagated in the various models. A rigorous comparison of time-evolving surfaces should thus be based on identical sets of (random or deterministic) initial phases. However, such phases can only be prescribed for linear surfaces but not for Lagrangian or HOS surfaces, which undergo a nonlinear transformation. To mitigate possible discrepancies arising from the choice of initial phases, the HOS model is initialized with an explicit nonlinear solution, which is close to the Lagrangian solution (Perignon *et al.* 2010; Perignon 2011), namely the second-order Eulerian Stokes solution for irregular wave fields as detailed in Longuet-Higgins (1963). The same underlying linear surface can be used to generate Lagrangian surfaces in the second-order expansions (CWM2, ICWM), through a geometrical transformation based on the Hilbert Transform.

5.2. Periodic Waves

Let us first consider a strongly nonlinear periodic wave of steepness $H/\lambda \simeq 0.08$ and period T , where $H = 2a$ is the wave height and λ the wavelength; for linear deep water waves, $T = \sqrt{2\pi\lambda/g}$. This steepness is over half the deep water limiting steepness and corresponds to $ka \simeq 0.25$, which is in the domain of applicability of the Lagrangian approach (Pierson 1961). For periodic waves, free surfaces represented in the various models can be easily synchronized at initial time, using the same phase as that of the fundamental component of the HOS solution. A domain of length equal to one wavelength is used to evaluate the error.



(a)



(b)

FIGURE 2. Comparison of results computed for a periodic wave of steepness $H/\lambda \simeq 8\%$, with the HOS (—), linear (⋯), CWM2 (---), and ICWM (-.-) models: (a) Error as a function of time with respect to the HOS solution; (b) normalized free surface elevations after approximately four periods of propagation.

Fig. 2a shows that, at $t = 0$, the CWM2 and ICWM surface elevations are identical since time dependent terms vanish. Both solutions also match quite well the HOS solution (very small errors can be seen in the figure), and much better than the linear solution, whose error is $\epsilon_{\text{LAG}}(0) \simeq 0.15$, due to an inaccurate wave shape. In Fig. 2a, the errors for the CWM2 and linear model follow a parallel growth: while the linear wave does not experience nonlinear phase velocity corrections, CWM2 is penalized by an overestimated nonlinear correction (close to twice the correct value, as discussed in Section 2). By contrast, for ICWM, the improved estimate of the nonlinear phase shift allows for errors to remain very small throughout the four-period propagation time considered here. At this stage, Fig. 2b shows a very marked phase shift of the linear and CWM2 model results with respect to the HOS reference solution, whereas no measurable shift is seen for the ICWM solution.

5.3. Irregular Waves

The performance of the improved Lagrangian formulation is now assessed for irregular waves generated on the basis of a specified energy density spectrum $S(\omega)$ (see Fig. 3).

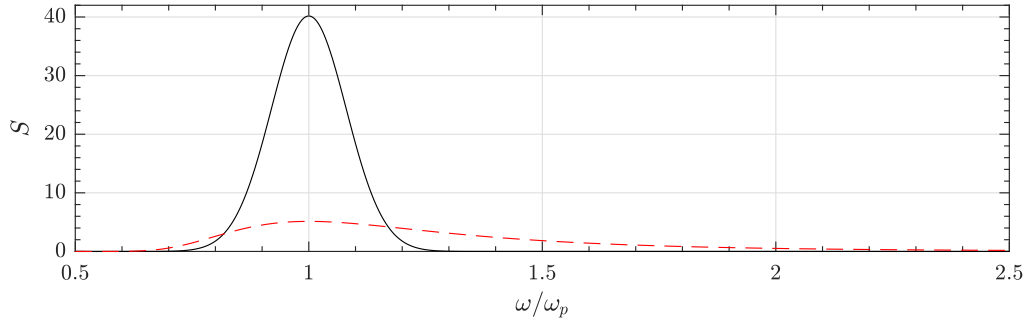


FIGURE 3. Energy density spectrum as a function of the dimensionless angular frequency ω/ω_p , for a narrow (Gauss, solid line) or broad-banded (JS, red dashed line) spectrum. The characteristic steepness is $H_s/\lambda_p \simeq 6\%$ and 4% for each case, respectively.

Similar to the periodic wave case, we investigate the time evolution of the error of the CWM2, ICWM, and linear solution, with respect to the HOS reference solution. Given a sea state of parameters (H_s, T_p) , the influence of energy spreading around the peak spectral frequency on the performance of the various wave models is investigated by considering two different spectra: (i) a narrow-banded Gaussian spectrum:

$$S(\omega) = \alpha \frac{1}{\sqrt{2\pi}\sigma^2} e^{-\frac{(\omega-\omega_p)^2}{2\sigma^2}}, \quad (5.5)$$

of standard deviation $\sigma/\omega_p = 0.08$, where $\omega_p = 2\pi/T_p$ denotes the peak angular frequency, and (ii) a JONSWAP (JS) spectrum with peakedness parameter $\gamma = 1$:

$$S(\omega) = \alpha \frac{g^2}{\omega^5} e^{-\frac{5}{4}(\frac{\omega_p}{\omega})^4} \quad (5.6)$$

(i.e., similar to the Pierson-Moskowitz (PM) spectrum of a fully developed sea, but with fetch-dependent peak frequency). In both cases, parameter α is found based on a specified H_s value, from the standard definition:

$$\int_0^\infty S(\omega) d\omega = \frac{H_s^2}{16} \quad (5.7)$$

In the applications, we use $T_p = 10$ s with $H_s = 9$ m for the Gaussian spectrum and $H_s = 6$ m for the JS spectrum. This yields characteristic deep water steepnesses $H_s/\lambda_p \simeq 6\%$ and 4% , respectively, with $\lambda_p = 2\pi/k_p$ denoting the peak spectral wavelength (note that the corresponding PM spectrum would have $T_p = 12.3$ s, i.e., the JS spectrum used here represents a fetch limited sea). The corresponding spectra are shown in Fig. 3.

For irregular waves, a larger number of dominant waves than in the periodic case must be modeled in the computational domain, in order to achieve convergence of the integral error of Eq. (5.2); here we use a spatial domain spanning eight peak wavelengths, i.e., $L = 8\lambda_p$. At $t = 0$, the linear and CWM free surfaces are constructed from the linear spectral information using the same set of random phases. For the HOS model, however, unlike periodic waves, linear information cannot be retrieved (except at initialization time $t = 0$) due to the implicit nonlinear components. Moreover, using linear information to initialize the HOS nonlinear propagation would lead to unstable calculations of higher-order terms (Dommermuth 2000). Hence, to allow for a deterministic comparison between models, the HOS was initialized solver with a nonlinear irregular wave field, here, a second-order Stokes wave solution, following the method detailed in Perignon *et al.* (2010) and Perignon (2011).

Figure 4 shows the comparison of normalized surface elevations computed in the different models at $t = 4T_p$, for the two types of spectra. For the wave train extracted from a Gaussian spectrum, Fig. 4a shows that the ICWM model prediction remains very accurate after $4T_p$. With the other models, for which wave celerity is inaccurate, waves are either delayed (linear solution) or too fast (CWM2), with respect to the HOS reference solution. Similar observations can be made in Fig. 4b, although in a less obvious way, for waves extracted from a JS spectrum: after $4T_p$ of propagation, the overall locations of dominant waves modeled with the ICWM model are consistent with the HOS solution (although not their smaller fluctuations), whereas the linear and CWM2 solutions are already desynchronized with it.

More specifically, Figure 5 shows the time evolution of relative errors computed with Eq. (5.2) over the first 10 peak periods of propagation, for the two cases of Fig. 4. In the Gaussian spectrum case, the ICWM model yields errors reduced by a factor of ~ 2 with respect to the linear solution as well as a significant improvement with respect to results of the CWM2 model. The overall error is larger in the JS spectrum case, but the same qualitative observations hold true. To quantify the effect of second-order interaction terms, which have been discarded in the ICWM model to obtain a numerically efficient solution, the CWM2 model results with a corrected dispersion relationship (4.19) have also been computed (referred to as ‘‘ICWM with interaction terms’’ in Fig. 5). As seen in the figures, these terms only yield significant effects within the first peak period of propagation (particularly in the Gaussian case) and become rapidly negligible with respect to the correction due to the dispersion relationship (ICWM). The black lines in Fig. 5 show the relative variation of the wave energy spectrum of the HOS reference surface, which is verified to remain small with respect to the relative error between methods. This confirms that the improved accuracy of ICWM for wave prediction is essentially due to a corrected wave celerity rather than an accurate description of bound waves.

We also checked the relative importance of the horizontal displacement term \tilde{D}_1 in Eq. (4.20) with respect to the wave celerity correction; to do so, we simulated the evolving surface according to LWT (not shown here), but using the corrected nonlinear dispersion relationship (i.e., Eq. (4.23) with $\tilde{D}_1 = 0$), a model henceforth referred to as LWT-CDR. At initial time, when it represents a purely linear surface, LWT-CDR yields a significantly larger relative error than ICWM (as can be seen in Figs. 2 and 5 at $t = 0$). However, after a few peak periods of propagation, we find that the LWT-CDR and ICWM solutions yield comparable errors, showing once again that, as far as predicting surface elevations, the dominant source of error is inaccuracies in wave celerity.

Note that numerical results are only shown in Fig. 5 for a single steepness for each spectrum (6% or 4%), which in fact represents the largest value achievable with the HOS model. At larger steepnesses, this model breaks down after a few periods due to the occurrence of wave breaking in the simulated sea-state, which is not explicitly treated in the version of HOS-ocean used in this study (Ducrozet *et al.* 2017). We performed a more systematic numerical investigation of the effect of wave steepness, which showed as could be expected that gradually increasing it both increases discrepancies between the linear and nonlinear model results and yields larger errors as time increases. For small steepness, the effect of interaction terms is negligible while the divergence of the linear model is still significant in the long term.

An important final remark is that criterion (5.2), used to quantify the error with respect to a rigorous model, is based on the RMS of surface elevations, which is mostly impacted by long waves. However, when it comes to predicting or interpreting properties of radar or LIDAR beams scattered by the sea surface, the accurate description of the

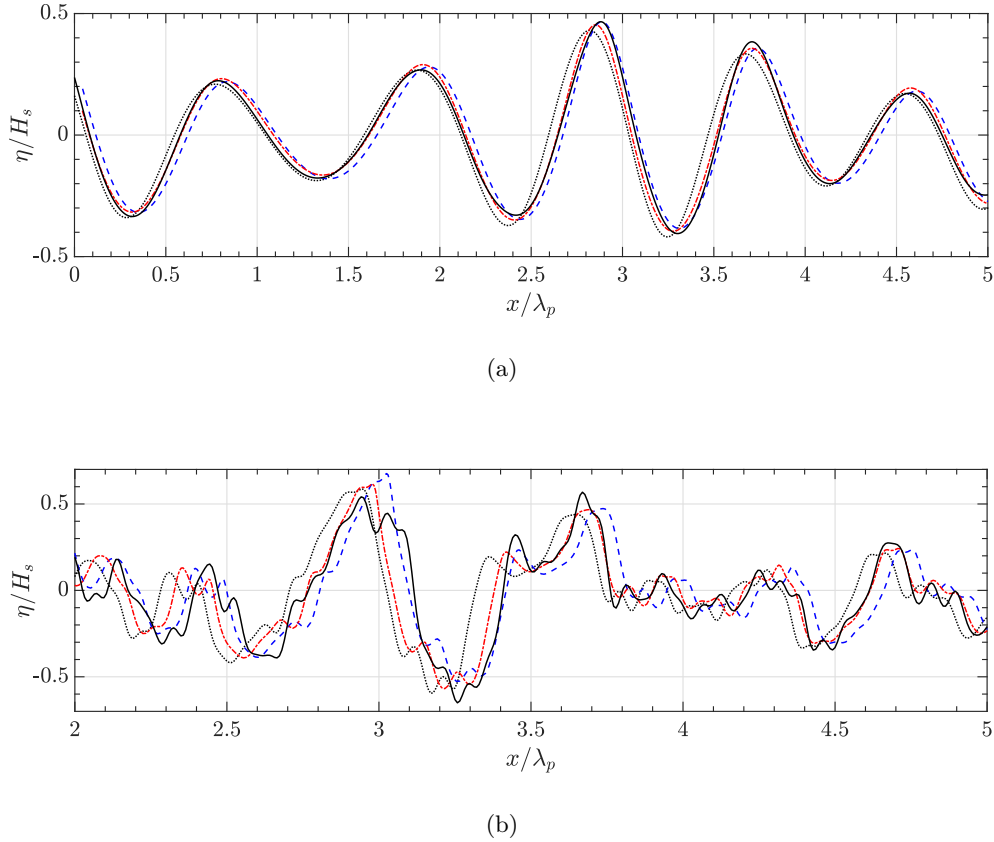
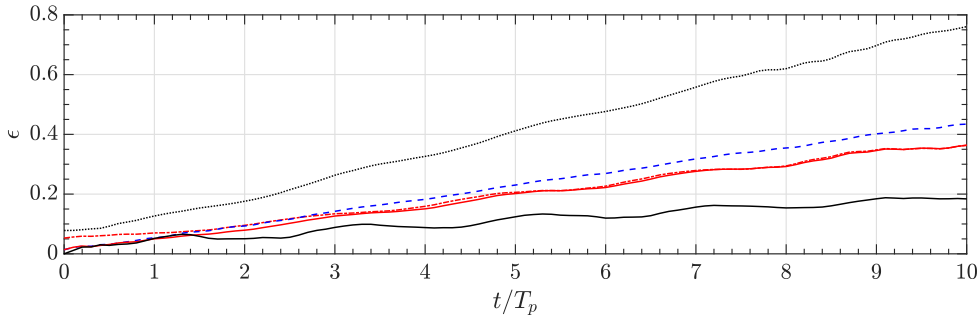


FIGURE 4. Normalized surface elevations computed with: HOS (—), linear (.....), CWM2 (---), and ICWM (-.-.) models, after $t = 4T_p$ of propagation, for irregular wave trains with $T_p = 10$ s extracted from a: (a) Gaussian spectrum with standard deviation $\sigma/\omega_p = 0.08$, $H_s = 9$ m, and characteristic steepness $H_s/\lambda_p \simeq 6\%$; and (b) a JS spectrum with peakedness parameter $\gamma = 1$ (similar to a PM spectrum), $H_s = 6$ m, and $H_s/\lambda_p \simeq 4\%$. See Fig. 3 for spectral shapes.

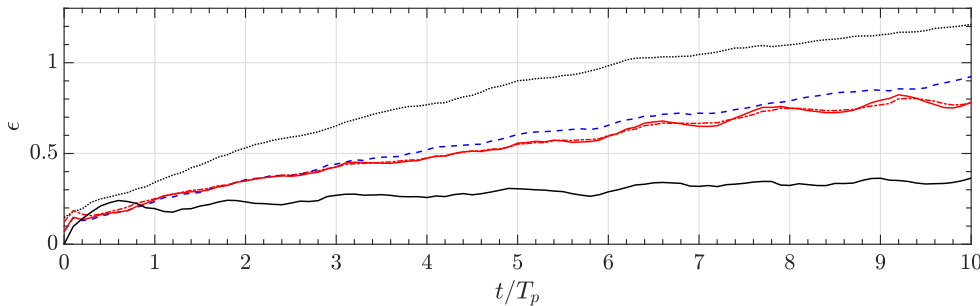
free surface roughness at small scale becomes crucial. In this context, the improvement of the ICWM over LWT or LWT-CDR models is not only related to its kinematical correction (which was found to be dominant in the present numerical analyses), but also to its geometrical correction of wave shape, which more significantly affects free surface slopes. Additional work is in progress to evaluate the performance of the ICWM from this “small scale roughness” point of view.

6. Discussion and conclusion

In this paper we derived and validated an improved and numerically efficient Lagrangian surface wave model, referred to as ‘Improved Choppy Wave Model’ (ICWM), derived by correcting a conceptual flaw in the classical Lagrangian expansion, namely an inappropriate choice of the reference particle location that leads to increasing errors as waves propagate. We presented a simplified approach for deriving Lagrangian solutions, based on iteratively solving the dynamical system relating water particle locations to



(a)



(b)

FIGURE 5. Time evolution of relative errors (Eq. (5.2)) for the two cases of Fig. 4 (a and b), for the linear (.....), CWM2 (-.-.-), ICWM (-.-.-) and ICWM with interaction terms (—) model results. The black solid line shows the relative change (Eq. (5.4)) of the prescribed spectrum during the HOS time evolution.

the Eulerian velocity field. Doing so, we could formally recover, in a much simpler way, the classical second-order Lagrangian expansion (CWM2) derived in the literature based on first-principles (Nouguier *et al.* 2015). One major difference with CWM2, however, is that ICWM uses a modified, more accurate, dispersion relationship that accounts for amplitude dispersion effects consistent with a third-order Eulerian expansion (Dean & Dalrymple 1991). The numerically efficient version of the ICWM model was obtained by discarding complex second-order interaction terms arising in the complete expansion, but keeping the dominant second-order effects, namely Stokes drift and mean sea level (MSL) correction. We showed that the neglected terms were not necessary to achieve a good solution in the short term. The model accuracy and efficiency were numerically assessed for 2D-surfaces, by performing a systematic comparison of different model solutions (linear wave theory (LWT), CWM2 and ICWM) with that of a fully non linear Higher-Order Spectral (HOS) model. We found that using ICWM led to a significant improvement of phased-resolved wave propagation, up to a few dominant wave periods of propagation, at a significantly reduced computational cost compared to using CWM2. A model based on LWT, but using the same corrected dispersion relationship (CDR) as

ICWM, referred to as LWT-CDR, achieved nearly the same accuracy as ICWM after a few periods of propagation, confirming that the CDR is the most important factor for obtaining an accurate solution. However, since the computational cost of using LWT-CDR is about the same as ICWM, the latter model, which more accurately accounts for the geometry of nonlinear waves, is still preferred.

ACKNOWLEDGMENT This work was supported by the Naval Group and Centrale Nantes, through their Joint Laboratory for Marine Technology, and by the PREDEMO-NAV project, grant ANR-15-ASTR-0006.

REFERENCES

- ASC 2018 Flash LIDAR™, <http://www.advancedscientificconcepts.com/products/overview.html>, Advanced Scientific Concepts Inc., Santa Barbara, CA, USA.
- BABARIT, AURÉLIEN & CLÉMENT, ALAIN 2006 Optimal latching control of a wave energy device in regular and irregular waves. *Applied Ocean Research* **28** (2), 77–91.
- BELMONT, MR, HORWOOD, JMK, THURLEY, RWF & BAKER, J 2007 Shallow angle wave profiling LIDAR. *Journal of Atmospheric and Oceanic Technology* **24** (6), 1150–1156.
- BLONDEL-COUPRIE, E., BONNEFOY, F. & FERRANT, P. 2013 Experimental validation of nonlinear deterministic prediction schemes for long-crested waves. *Ocean Engineering* **58**, 284–292.
- BONNEFOY, F., DUCROZET, G., LE TOUZÉ, D. & FERRANT, P., ed. 2009 *Advances in Numerical Simulation of Nonlinear Water Waves, Advances in Coastal and Ocean Engineering*, vol. 11, Chap. Time-Domain Simulation of Nonlinear Water Waves Using Spectral Methods, pp. 129–164. World Scientific.
- CLAMOND, DIDIER 2007 On the Lagrangian description of steady surface gravity waves. *Journal of Fluid Mechanics* **589**, 433–454.
- DANKERT, H & ROSENTHAL, W 2004 Ocean surface determination from X-band radar-image sequences. *Journal of Geophysical Research: Oceans* **109** (C4).
- DANNENBERG, JENS, HESSNER, KATRIN, NAAIJEN, PETER, VAN DEN BOOM, HENK, REICHERT, KONSTANZE *et al.* 2010 The on board wave and motion estimator OWME. In *The 20th International Offshore and Polar Engineering Conference*. International Society of Offshore and Polar Engineers.
- DEAN, ROBERT G & DALRYMPLE, ROBERT A 1991 *Water wave mechanics for engineers and scientists*, , vol. 2. world scientific publishing Co Inc.
- DOMMERMUTH, DOUGLAS 2000 The initialization of nonlinear waves using an adjustment scheme. *Wave Motion* **32** (4), 307–317.
- DOMMERMUTH, DOUGLAS G. & YUE, DICK K. P. 1987 A high-order spectral method for the study of nonlinear gravity waves. *Journal of Fluid Mechanics* **184**, 267–288.
- DUCROZET, G., BONNEFOY, F., LE TOUZÉ, D. & FERRANT, P. 2007 3-d hos simulations of extreme waves in open seas. *Natural Hazards and Earth System Sciences* **7**, 109–122.
- DUCROZET, G., BONNEFOY, F., LE TOUZÉ, D. & FERRANT, P. 2016 Hos-ocean: Open-source solver for nonlinear waves in open ocean based on high-order spectral method. *Computer Physics Communications* **203**, 245–254.
- DUCROZET, GUILLAUME, BONNEFOY, FÉLICIEEN & PERIGNON, YVES 2017 Applicability and limitations of highly non-linear potential flow solvers in the context of water waves. *Ocean Engineering* **142**, 233–244.
- FENTON, JOHN D 1985 A fifth-order stokes theory for steady waves. *Journal of waterway, port, coastal, and ocean engineering* **111** (2), 216–234.
- GERSTNER, FJ 1809 Theorie der Wellen. *Annalen der Physik* **32** (8), 412–445.
- GRILLI, STÉPHAN T, GUÉRIN, CHARLES-ANTOINE & GOLDSTEIN, BART 2011 Ocean wave reconstruction algorithms based on spatio-temporal data acquired by a Flash LIDAR camera. In *The 21st International Offshore and Polar Engineering Conference*, pp. 275–282. International Society of Offshore and Polar Engineers.

- HILMER, TYSON & THORNHILL, ERIC 2014 Deterministic wave predictions from the wamos ii. In *OCEANS 2014-TAIPEI*, pp. 1–8. IEEE.
- LINDGREN, GEORG 2009 Exact asymmetric slope distributions in stochastic gauss–lagrange ocean waves. *Applied Ocean Research* **31** (1), 65–73.
- LINDGREN, GEORG 2010 Slope distribution in front-back asymmetric stochastic lagrange time waves. *Advances in Applied Probability* **42** (2), 489–508.
- LINDGREN, GEORG 2015 Asymmetric waves in wave energy systems analysed by the stochastic gauss–lagrange wave model. *Proceedings of the Estonian Academy of Sciences* **64** (3), 291.
- LINDGREN, GEORG & ÅBERG, SOFIA 2009 First order stochastic lagrange model for asymmetric ocean waves. *Journal of Offshore Mechanics and Arctic Engineering* **131** (3), 031602.
- LONGUET-HIGGINS, MICHAEL S 1963 The effect of non-linearities on statistical distributions in the theory of sea waves. *Journal of fluid mechanics* **17** (3), 459–480.
- MONISMITH, S. G., COWEN, E. A., NEPF, H. M., MAGNAUDET, J. & THAIS, L. 2007 Laboratory observations of mean flows under surface gravity waves. *Journal of Fluid Mechanics* **573**, 131–147.
- NAAIJEN, PETER, VAN OOSTEN, KEES, ROOZEN, KAREL & VAN’T VEER, RIAAN 2018 Validation of a deterministic wave and ship motion prediction system. In *ASME 2018 37th International Conference on Ocean, Offshore and Arctic Engineering*. American Society of Mechanical Engineers.
- NIETO BORGE, JOSÉ C, RODRÍGUEZ, GERMÁN RODRÍGUEZ, HESSNER, KATRIN & GONZÁLEZ, PALOMA IZQUIERDO 2004 Inversion of marine radar images for surface wave analysis. *Journal of Atmospheric and Oceanic Technology* **21** (8), 1291–1300.
- NOUGUIER, FRÉDÉRIC, CHAPRON, BERTRAND & GUÉRIN, CHARLES-ANTOINE 2015 Second-order lagrangian description of tri-dimensional gravity wave interactions. *Journal of Fluid Mechanics* **772**, 165–196.
- NOUGUIER, FRÉDÉRIC, GRILLI, STÉPHAN T & GUÉRIN, CHARLES-ANTOINE 2014 Nonlinear ocean wave reconstruction algorithms based on spatiotemporal data acquired by a Flash LIDAR camera. *IEEE Transactions on Geoscience and Remote Sensing* **52** (3), 1761–1771.
- NOUGUIER, FRÉDÉRIC, GUÉRIN, CHARLES-ANTOINE & CHAPRON, BERTRAND 2009 ‘Choppy wave’ model for nonlinear gravity waves. *Journal of Geophysical Research: Oceans* **114** (C9).
- PEREZ, TRISTAN 2006 *Ship motion control: course keeping and roll stabilisation using rudder and fins*. Springer Science & Business Media.
- PERIGNON, YVES 2011 Modélisation déterministe des états de mer-application à la rétrodiffusion d’ondes radar. PhD thesis, Ecole Centrale de Nantes (ECN).
- PERIGNON, YVES L, BONNEFOY, FELICIEN, FERRANT, PIERRE & DUCROZET, GUILLAUME 2010 Non-linear initialization in three-dimensional high order spectra deterministic sea state modeling. In *ASME 2010 29th International Conference on Ocean, Offshore and Arctic Engineering*, pp. 525–532. American Society of Mechanical Engineers.
- PIERSON, WJ 1961 Models of random seas based on the lagrangian equations of motion. *Tech. Rep.*. New York Univ., Coll. of Eng. Res. Div., Dept. of Meteorology and Oceanography, tech. Rep. prepared for the Office of Naval Research under contract Nonr-285(03).
- PIERSON, WJ 1962 Perturbation analysis of the Navier–Stokes equations in Lagrangian form with selected linear solutions. *J. Geophys. Res* **67** (8), 3151–3160.
- QI, YUSHENG, WU, GUANGYU, LIU, YUMING, KIM, MOO-HYUN & YUE, DICK K. P. 2018a Nonlinear phase-resolved reconstruction of irregular water waves. *Journal of Fluid Mechanics* **838**, 544–572.
- QI, YUSHENG, WU, GUANGYU, LIU, YUMING & YUE, DICK KP 2018b Predictable zone for phase-resolved reconstruction and forecast of irregular waves. *Wave Motion* **77**, 195–213.
- QI, YUSHENG, XIAO, WENTING & YUE, DICK KP 2016 Phase-resolved wave field simulation calibration of sea surface reconstruction using noncoherent marine radar. *Journal of Atmospheric and Oceanic Technology* **33** (6), 1135–1149.
- WEST, BRUCE J., BRUECKNER, KEITH A., JANDA, RALPH S., MILDER, D. MICHAEL & MILTON, ROBERT L. 1987 A new numerical method for surface hydrodynamics. *Journal of Geophysical Research: Oceans* **92** (C11), 11803–11824.

7. Appendix: Three-dimensional irregular waves

The generalization of the technique to three dimensions (3D) is straightforward, although more algebra is involved. Below, we only provide the main steps in the calculations. The 3D linearized solution for the surface elevation reads:

$$\eta_1(x, y, t) = \sum_{i=1}^N a_i \cos \psi_i \quad (7.1)$$

where $\psi_i = \mathbf{k}_i \cdot \mathbf{r} - \omega_i t - \varphi_i$, $\mathbf{r} = (x, y)$, $\mathbf{k}_i = (k_{ix}, k_{iy})$, $k_i = \|\mathbf{k}_i\|$ and $\omega_i = \sqrt{gk_i}$. The corresponding linearized solution for the velocity field is given by:

$$\begin{aligned} U^{(1)}(x, y, z, t) &= \sum_{i=1}^N a_i \omega_i \frac{k_{ix}}{k_i} e^{k_i z} \cos \psi_i \\ V^{(1)}(x, y, z, t) &= \sum_{i=1}^N a_i \omega_i \frac{k_{iy}}{k_i} e^{k_i z} \cos \psi_i \\ W^{(1)}(x, y, z, t) &= \sum_{i=1}^N a_i \omega_i e^{k_i z} \sin \psi_i \end{aligned} \quad (7.2)$$

The expression of the second-order correction can again be found in Longuet-Higgins (1963) (through the velocity potential given p 466):

$$\phi^{(2)}(x, y, z, t) = \sum_{i,j} a_i a_j \left(A_{ij}^- e^{|\mathbf{k}_i - \mathbf{k}_j|z} \sin(\psi_i - \psi_j) + A_{ij}^+ e^{|\mathbf{k}_i + \mathbf{k}_j|z} \sin(\psi_i + \psi_j) \right) \quad (7.3)$$

where,

$$A_{ij}^{\pm} = \frac{\omega_i \omega_j}{k_i k_j} \frac{(\omega_i \mp \omega_j)(\mathbf{k}_i \cdot \mathbf{k}_j \pm k_i k_j)}{(\omega_i \mp \omega_j)^2 - g|\mathbf{k}_i \mp \mathbf{k}_j|} \quad (7.4)$$

Similar to the 2D case, the developments start from the dynamical system linking the particle locations:

$$\begin{aligned} X(t) &= \bar{x} + x_1(t) + x_2(t), \\ Y(t) &= \bar{y} + y_1(t) + y_2(t), \\ Z(t) &= \bar{z} + z_1(t) + z_2(t) \end{aligned} \quad (7.5)$$

to the Eulerian velocity field (U, V, W) , in which a second-order Taylor series expansion of the former around their mean locations $(\bar{x}, \bar{y}, \bar{z}) = (\bar{\mathbf{r}}, \bar{z})$ is expressed as:

$$\begin{aligned} \dot{\bar{x}}(t) &= U^{(1)}(\bar{\mathbf{r}}, \bar{z}, t) + U^{(2)}(\bar{\mathbf{r}}, \bar{z}, t) + \left\{ x(t) \frac{\partial U^{(1)}}{\partial x} + y(t) \frac{\partial U^{(1)}}{\partial y} + z(t) \frac{\partial U^{(1)}}{\partial z} \right\}(\bar{\mathbf{r}}, \bar{z}, t) \\ \dot{\bar{y}}(t) &= V^{(1)}(\bar{\mathbf{r}}, \bar{z}, t) + V^{(2)}(\bar{\mathbf{r}}, \bar{z}, t) + \left\{ x(t) \frac{\partial V^{(1)}}{\partial x} + y(t) \frac{\partial V^{(1)}}{\partial y} + z(t) \frac{\partial V^{(1)}}{\partial z} \right\}(\bar{\mathbf{r}}, \bar{z}, t) \\ \dot{\bar{z}}(t) &= W^{(1)}(\bar{\mathbf{r}}, \bar{z}, t) + W^{(2)}(\bar{\mathbf{r}}, \bar{z}, t) + \left\{ x(t) \frac{\partial W^{(1)}}{\partial x} + y(t) \frac{\partial W^{(1)}}{\partial y} + z(t) \frac{\partial W^{(1)}}{\partial z} \right\}(\bar{\mathbf{r}}, \bar{z}, t) \end{aligned} \quad (7.6)$$

The first-order contribution can easily be identified and integrated:

$$x_1(t) = - \sum_{i=1}^N a_i \frac{k_{ix}}{k_i} e^{k_i z} \sin \bar{\psi}_i; \quad y_1(t) = - \sum_{i=1}^N a_i \frac{k_{iy}}{k_i} e^{k_i z} \sin \bar{\psi}_i; \quad z_1(t) = \sum_{i=1}^N a_i e^{k_i z} \cos \bar{\psi}_i. \quad (7.7)$$

Again, the first-order solution given by Eqs. (7.5) and (7.7) is identical to the three-dimensional CWM of Noguier *et al.* (2009). Building on this solution, we easily obtain the following expressions for the time derivatives of second-order fluctuations:

$$\begin{aligned}
\dot{x}_2(t) &= \sum_{i,j} a_i a_j \left(A_{ij}^- e^{|\mathbf{k}_i - \mathbf{k}_j|z} (k_{ix} - k_{jx}) \cos(\bar{\psi}_i - \bar{\psi}_j) + A_{ij}^+ e^{|\mathbf{k}_i + \mathbf{k}_j|z} (k_{ix} + k_{jx}) \right. \\
&\quad \left. \cos(\bar{\psi}_i + \bar{\psi}_j) \right) + \sum_{i,j} a_i a_j k_{jx} \omega_j e^{(k_i + k_j)Z} \left(\frac{\mathbf{k}_i \cdot \mathbf{k}_j}{k_i k_j} \sin \bar{\psi}_i \sin \bar{\psi}_j + \cos \bar{\psi}_i \cos \bar{\psi}_j \right) \\
\dot{y}_2(t) &= \sum_{i,j} a_i a_j \left(A_{ij}^- e^{|\mathbf{k}_i - \mathbf{k}_j|z} (k_{iy} - k_{jy}) \cos(\bar{\psi}_i - \bar{\psi}_j) + A_{ij}^+ e^{|\mathbf{k}_i + \mathbf{k}_j|z} (k_{iy} + k_{jy}) \right. \\
&\quad \left. \cos(\bar{\psi}_i + \bar{\psi}_j) \right) + \sum_{i,j} a_i a_j k_{jy} \omega_j e^{(k_i + k_j)Z} \left(\frac{\mathbf{k}_i \cdot \mathbf{k}_j}{k_i k_j} \sin \bar{\psi}_i \sin \bar{\psi}_j + \cos \bar{\psi}_i \cos \bar{\psi}_j \right) \\
\dot{z}_2(t) &= \sum_{i,j} a_i a_j \left(A_{ij}^- e^{|\mathbf{k}_i - \mathbf{k}_j|z} |\mathbf{k}_i - \mathbf{k}_j| \sin(\bar{\psi}_i - \bar{\psi}_j) + A_{ij}^+ e^{|\mathbf{k}_i + \mathbf{k}_j|z} |\mathbf{k}_i + \mathbf{k}_j| \right. \\
&\quad \left. \sin(\bar{\psi}_i + \bar{\psi}_j) \right) + \sum_{i,j} a_i a_j k_j \omega_j e^{(k_i + k_j)Z} \left(\frac{\mathbf{k}_i \cdot \mathbf{k}_j}{k_i k_j} \sin \bar{\psi}_i \cos \bar{\psi}_j + \cos \bar{\psi}_i \sin \bar{\psi}_j \right)
\end{aligned} \tag{7.8}$$

Integrating Eqs. (7.8) as was done in the 2D case, yields the complete 3D Lagrangian solution (CWM2), which was already derived by Noguier *et al.* (2015) and, hence, is not detailed here. Instead, we concentrate on the numerically efficient second-order solution, using a corrected dispersion relationship. Hence, excluding interaction terms from the complete second-order formulation, we retain the free surface Stokes drift vector:

$$\mathbf{U}_{s0} = \sum_{i=1}^N a_i^2 \omega_i \mathbf{k}_i \tag{7.9}$$

and, with a straightforward generalization of the technique used in 2D, we find the modified angular frequency:

$$\tilde{\omega}_i = \omega_i - \frac{1}{2} \mathbf{k}_i \cdot \mathbf{U}_{s0} \tag{7.10}$$

Based on Eqs. (7.9) and (7.10), the Lagrangian evolution of the surface elevation is given by the 3D-ICWM as:

$$\begin{aligned}
\mathbf{r}(t) &= \mathbf{r}_0 - \sum_{i=1}^N a_i \frac{\mathbf{k}_i}{k_i} \sin \tilde{\psi}_i + \mathbf{U}_{s0} t \\
Z(t) &= \sum_{i=1}^N a_i \sin \tilde{\psi}_i + \frac{1}{2} \sum_{i=1}^N a_i^2 k_i, \\
\tilde{\psi}_i &= \mathbf{k}_i \cdot \mathbf{r} - \tilde{\omega}_i t - \varphi_i
\end{aligned} \tag{7.11}$$

whose efficient numerical solution can be developed following the same procedure as used in 2D, based on two-dimensional FFTs.